International Journal of Extreme Manufacturing

PAPER • **OPEN ACCESS**

Controllable rectification on the thermal conductivity of porous $YBa_2Cu_3O_{7-x}$ superconductors from 3D-printing

To cite this article: Yanbin Ma *et al* 2023 *Int. J. Extrem. Manuf.* **5** 015001

OPEN ACCESS
IOP Publishing | IMMT
International Journal of Extreme Manufacturing
Int. J. Extrem. Manuf. 5 (2023) 015001 (10pp)
https://doi.org/10.1088/2631-7990/ac9f88

Controllable rectification on the thermal conductivity of porous $YBa_2Cu_3O_{7-x}$ superconductors from 3D-printing

Yanbin Ma[1,2], Baoqiang Zhang[1,2], Xingyi Zhang[1,2,*] and You-He Zhou[1,2]

[1] Key Laboratory of Mechanics on Disaster and Environment in Western China attached to the Ministry of Education of China, Lanzhou University, Lanzhou, Gansu 730000, People's Republic of China
[2] Department of Mechanics and Engineering Sciences, College of Civil Engineering and Mechanics, Lanzhou University, Lanzhou, Gansu 730000, People's Republic of China

E-mail: zhangxingyi@lzu.edu.cn

Received 30 March 2022, revised 24 May 2022
Accepted for publication 31 October 2022
Published 24 November 2022

Abstract

Superconducting $YBa_2Cu_3O_{7-x}$ (YBCO) bulks have promising applications in quasi-permanent magnets, levitation, etc. Recently, a new way of fabricating porous YBCO bulks, named direct-ink-writing (DIW) 3D-printing method, has been reported. In this method, the customized precursor paste and programmable shape are two main advantages. Here, we have put forward a new way to customize the YBCO 3D-printing precursor paste which is doped with Al_2O_3 nanoparticles to obtain YBCO with higher thermal conductivity. The great rheological properties of precursor paste after being doped with Al_2O_3 nanoparticles can help the macroscopic YBCO samples with high thermal conductivity fabricated stably with high crystalline and lightweight properties. Test results show that the peak thermal conductivity of Al_2O_3-doped YBCO can reach twice as much as pure YBCO, which makes a great effort to reduce the quench propagation speed. Based on the microstructure analysis, one can find that the thermal conductivity of Al_2O_3-doped YBCO has been determined by its components and microstructures. In addition, a macroscopic theoretical model has been proposed to assess the thermal conductivity of different microstructures, whose calculated results take good agreement with the experimental results. Meanwhile, a microstructure with high thermal conductivity has been found. Finally, a macroscopic YBCO bulk with the presented high thermal conductivity microstructure has been fabricated by the Al_2O_3-doped method. Compared with YBCO fabricated by the traditional 3D-printed, the Al_2O_3-doped structural YBCO bulks present excellent heat transfer performances. Our customized design of 3D-printing precursor pastes and novel concept of structural design for enhancing the thermal conductivity of YBCO superconducting material can be widely used in other DIW 3D-printing materials.

Keywords: Al_2O_3-doped YBCO, thermal conductivity, theoretical model, controllable design, DIW 3D-printing

* Author to whom any correspondence should be addressed.

2631-7990/23/015001+10$33.00

1. Introduction

High-temperature superconducting $YBa_2Cu_3O_{7-x}$ (YBCO) has become a popular superconducting material. Various kinds of phenomena in the physical properties of YBCO have been reported by research groups all over the world. The thermal conductivity of the oxide superconductors [1–5] is a physically important quantity that reflects the strength of the interaction between phonons and charge carries [6, 7]. Thermal conductivity k is a fundamental property needed to calculate thermal-magnetic instability and cooling energy, and thermal-induced quench is a common phenomenon that needs to be solved urgently. Jing *et al* numerically calculated the thermal-magnetic-mechanical instability behavior, and achieved some distinctive progresses for recognizing the mechanics and thermotics-relevant behaviors in bulk and film superconductors [8–12]. In the quench research of high-temperature superconducting materials, the main research parameters are the minimum quench trigger energy (MQE) and quench propagation velocity. When the superconductor is disturbed by energy during its operation, the superconducting materials and the environment cannot balance this energy, which will induce the superconductor to quench. The minimum energy that can just induce the superconductor to quench is called the MQE. The local position changes from a superconducting state to a normal state due to disturbance, and the Joule heat will be released at this position due to the appearance of resistance, which will lead to a sudden rise in local temperature. If this heat cannot be conducted away in time, the quench position will propagate along the current transmission direction, and the propagation speed in the normal state region is called quench propagation speed. Therefore, superconducting materials with higher thermal conductivity can reduce the quench propagation speed significantly, which leads to YBCO with high thermal conductivity becoming more promising. For these years, thermal conductivity measurements have been focused on the YBCO polycrystals [13–16], single crystals [17–19], YBCO thin film [20], and YBCO tape [21] for business. In conventional metals, the electrons are the main heat carriers, instead of phonons due to the test temperature being higher than the superconducting transition temperature [22]. The mechanism of thermal conductivity for YBCO materials has been elucidated by the theory of microscale about the interaction between phonons and electrons However, there is no macro model to illustrate the mechanism of thermal conductivity for macro-scale YBCO bulk materials.

As to YBCO bulks, Yamamoto *et al* [23] fabricated YBCO doped with and without Ag by the melt powdering melt growth (MPMG) method, and measured its thermal conductivity, respectively. They obtained thermal conductivity with a small temperature range and discussed the effect of the impurity phase briefly. Rodríguez [24] found that the thermal process and Ag doping do affect the charge-carrier density of these compounds directly by measuring the electrical resistivity, Seebeck coefficient and thermal conductivity. However, the fabricating process of YBCO is always using top seeded infiltration and growth method or MPMG method, which results in a long fabricating period and surface cracks on samples [25, 26]. The advanced additive manufacturing technology has the characteristics of high efficiency and nimble, as the prepared sample has better mechanical and thermal performances [27–29]. Recently, our research group has put forward a new YBCO bulk material fabricating process using the direct-ink-writing (DIW) 3D-printing method [30]. In this method, the rheological properties are the most important factors for the ceramic paste, which will directly determine its printability [31]. Meanwhile, the YBCO bulks with various kinds of complex structures have been easily fabricated. However, there has been no systematic research aiming at the thermal conductivity of doped DIW 3D-printing YBCO bulk materials.

In this paper, to enhance the thermal conductivity of YBCO bulks and to make it controllable simultaneously, the structural design method has been proposed based on a unique macro theoretic model of the thermal conductivity for YBCO combined with the DIW 3D-printing fabricating process. Based on DIW 3D-printing fabricating process, it is easier to add Al_2O_3 nanoparticles into the YBCO 3D-printing ink, which also contains Y_2O_3, $BaCO_3$ and CuO nanoparticles. The thermal conductivity of the Al_2O_3-enhanced YBCO bulk was larger than the pure YBCO bulk. To analyze the mechanism of thermal conductivity of enhanced YBCO, the macro-scale model has been constructed based on structure deformation, which can reveal the change of thermal conductivity with rising temperatures. Furthermore, a smart structure made of enhanced YBCO that contains higher thermal conductivity has been designed based on the DIW 3D-printing fabricating process, which has larger thermal conductivity than traditional 3D-printed YBCO.

2. Results and discussion

2.1. Preparation of Al_2O_3-doped YBCO bulks with larger thermal conductivity

The fabrication of YBCO bulks with larger thermal conductivity is based on the DIW 3D-printing process, which is shown in figure 1. To fabricate simple YBCO without doping, the Y_2O_3, $BaCO_3$ and CuO powders are needed, and their diameters are all less than 1 μm. We choose Al_2O_3 nanoparticles as doping material because it has higher thermal conductivity. Since Al_2O_3 nanoparticles do not react with Y_2O_3, $BaCO_3$ and CuO at the sintering temperature, the Al_2O_3 nanoparticles were added to the YBCO precursor powder mixture. The mechanism of Al_2O_3 particles enhanced YBCO with higher thermal conductivity is that Al_2O_3 and YBCO combined and became a composite material. Meanwhile, with Al_2O_3 doping into YBCO, the density of YBCO can be enhanced, which causes higher thermal conductivity of a composite material. To make the precursor powder mixture into the slurry required for 3D printing, it is first necessary to prepare a binder solution. Generally, sodium carboxymethyl cellulose ($RnOCH_2COONa$) and deionized water are mixed in a weight ratio (1:15). In a glass beaker, a mechanical stirring process was adopted at room temperature for at least 72 h to obtain a uniform water-based precursor. Then, the ground powder

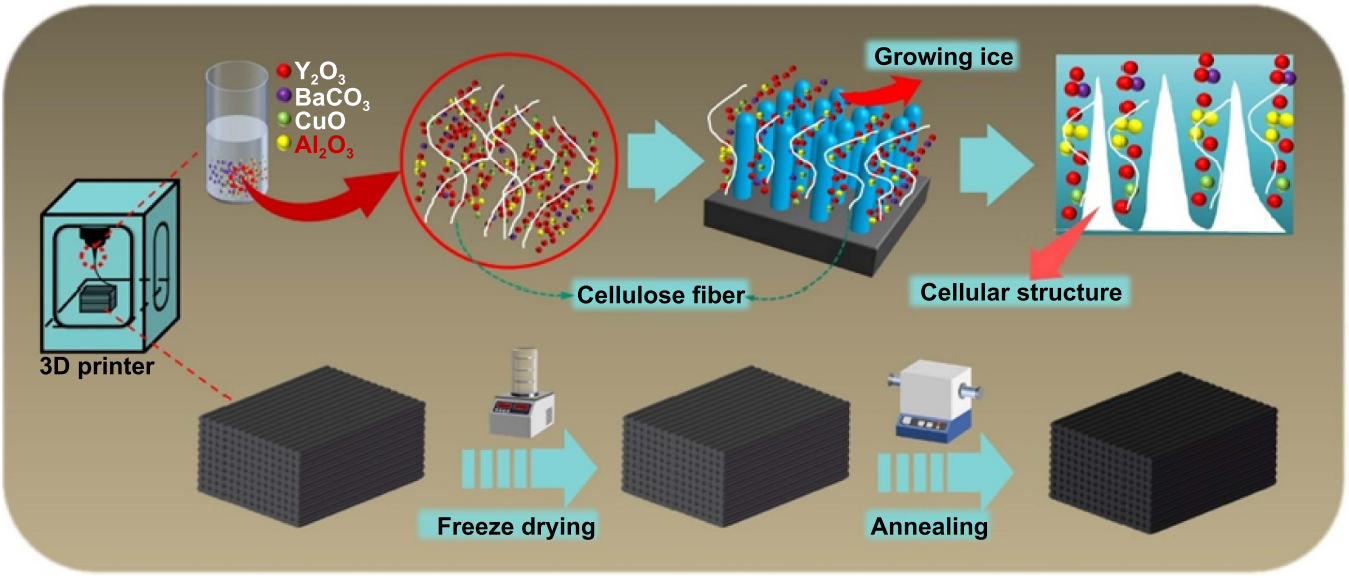

Figure 1. Fabrication of YBCO with larger thermal conductivity doped with Al_2O_3 by the 3D-printing method.

is fully dispersed into the water-based precursor in an agate mortar. After fully stirring, a two-phase system printing paste is obtained. For the three-phase paste slurry, soybean oil epoxide ($C_{57}H_{98}O_{12}$) was dissolved in the binder solution, and the oil–water–powder three-phase mixed suspension was obtained by stirring. To obtain better paste uniformity, a roller mill can also be used to homogenize the mixture between steel rollers. Finally, the printing paste with uniform elasticity and good performance is obtained. If the printed YBCO sample is dried directly, a large number of irregular circular cavities will be generated in the sample. However, when the 3D printed structure is processed in an ice-cold environment (−60 °C), as the water in the structure freezes, cellulose fibers that absorb numerous particles are gradually excluded from the growing ice crystals. Therefore, the distance between the fibers is reduced, forcing them to form interconnected reinforced scaffolds together, and after freeze-drying, because many mechanically reinforced scaffolds are formed in the structure, they can be strong enough to withstand crystallization migration at the interface of annealing liquid phase without large deformation. Therefore, the samples were freeze-dried at −50 °C for 48 h. At the same time, during the freeze-drying process, the extrusion of ice crystals improved the close contact between different particles and formed a good intracellular structure. In addition, this method can prevent the internal crack propagation of 3D-printed YBCO bulk caused by initial temperature difference and spatial anisotropy. After the freeze-drying, the YBCO samples were annealed at 920 °C in an oxygen atmosphere to enhance their thermal conductivity. After sintering, to make up for the lack of oxygen in YBCO bulk materials during the preparation process, the YBCO samples were annealed at 480 °C in 0.4 MPa oxygen pressure atmosphere, and finally, the fully prepared YBCO bulk materials can be obtained.

Fundamentally, the printability of ceramic precursor paste is determined by the rheological and thixotropic properties. Meantime, they also affect the structural stability and geometric accuracy of the 3D-printed samples [32].

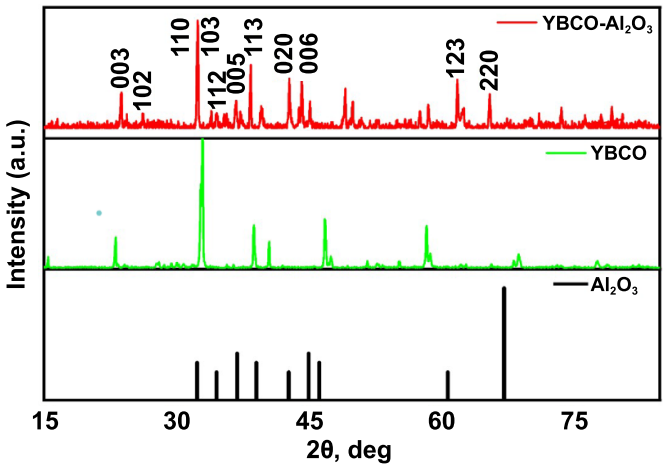

Figure 2. X-ray diffraction (XRD) of Al_2O_3-doped 3D-printed YBCO with high thermal conductivity, pure YBCO and pure Al_2O_3.

Researchers have proposed that the viscosity of 2000 Pa·s is suitable for fabricating stable constructions of the YBCO [33]. In our work, the weight ratio of epoxidized soybean oil and water has been changed prepared thermal conductivity precursor paste to make sure it can be well used to fabricate stable structures. Zhang *et al* [30] confirmed the best anneal temperature of samples is 920 °C which makes samples have higher crystallinity and uniform grain size. Therefore, our work also chooses 920 °C as anneal temperature to keep Al_2O_3-doped YBCO has the same properties as pure YBCO.

2.2. *Microstructure of Al_2O_3-doped 3D-printed YBCO bulk*

The chemical composition and structure of Al_2O_3-doped 3D-printed YBCO bulk with high thermal conductivity were further characterized by x-ray diffraction (XRD), as shown in figure 2. The XRD pattern of pure YBCO, pure Al_2O_3 and Al_2O_3-doped YBCO with high thermal conductivity all show

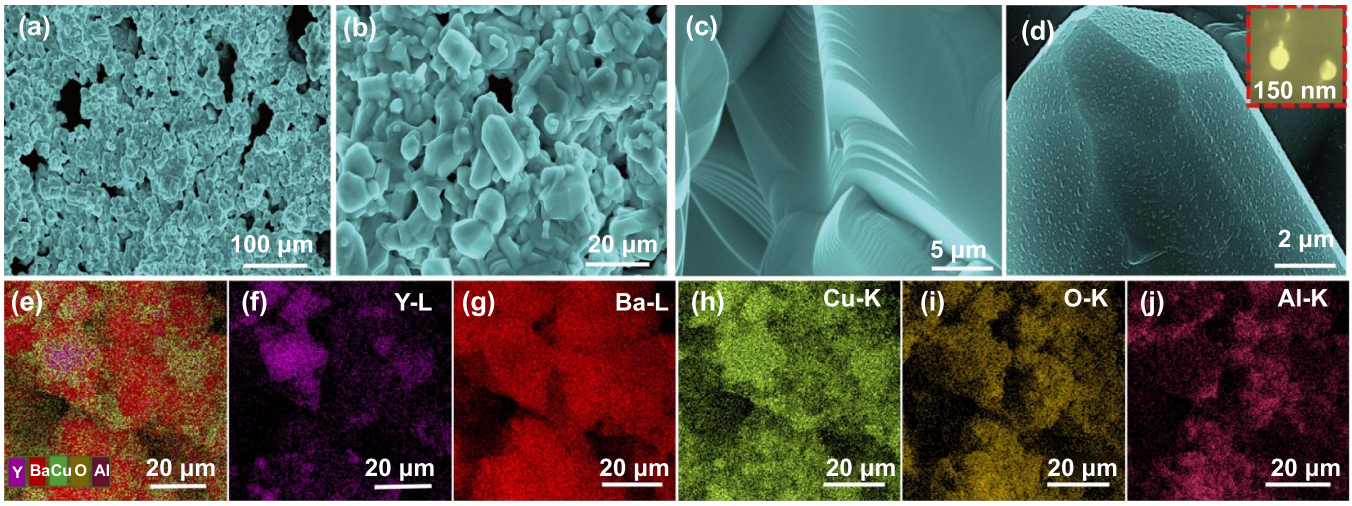

Figure 3. Microstructural characterization of Al_2O_3-doped thermal enhanced 3D-printed YBCO structure. (a)–(d) Scanning Electron Microscope (SEM) images of Al2O3 doped thermal enhanced 3D-printed YBCO structure. (e)–(j) Elemental mapping (Y, Ba, Cu, O, Al) images of Al_2O_3-doped 3D-printed YBCO sample with high thermal conductivity.

specific sharp peaks, which indicated the compositions of YBCO and Al_2O_3 nanoparticles. As shown in figures 3(a)–(c), the sintered Al_2O_3-doped YBCO with high thermal conductivity has a porous structure. According to figure 3(d), it is clear that Al_2O_3 nanoparticles had been doped in the YBCO structure homogeneously. Though the radius of Al_2O_3 nanoparticles was controlled at about 30 nm, the aggregation of the nanoparticles also appeared during the preparation of precursor paste and the freeze-drying process, which can be seen in the inset of figure 3(d). As shown in figures 3(e)–(j), corresponding to the synthesized elements, Y, Ba, Cu, O, and Al, respectively. According to these five elements' distribution's color mapping, Al_2O_3-doped YBCO with high thermal conductivity was confirmed to be fabricated successfully as an YBCO composite.

2.3. Superconducting properties of Al_2O_3-doped YBCO with high thermal conductivity

Al_2O_3 is a kind of nanoparticle with high thermal conductivity. In this paper, we use Al_2O_3nanoparticles to improve the thermal conductivity of YBCO bulk materials for 3D-printing. Like 3D printed YBCO superconducting bulk materials, we tested the superconducting properties of bulk materials doped with alumina nanoparticles and measured the temperature dependence and magnetic field intensity of magnetization of 3D printed YBCO doped with Al_2O_3 nanoparticles by using a magnetic measuring system.

Critical current density (J_c, A cm^{-2}) is an important evaluation index of superconductivity, which is calculated from the M–Ba curve by using Bean-model's formula [34]:

$$J_c = \frac{20\Delta M}{b(1 - b/3a)} \quad (1)$$

where ΔM is the width of the magnetized hysteresis loop (emu cm^{-3}), a and b ($a > b$) are the cross-sectional dimensions of the sample perpendicular to the magnetic field, respectively.

Figures 4(a)–(c) show graphs of magnetization versus magnetic field (from −90 kOe to 90 kOe) of 3D printed samples doped with different Al_2O_3 ratios with temperatures ranging from 2.5 K to 55 K. With different Al_2O_3 doping ratios, the YBCO superconducting properties show giant differences, which indicated that the sample doped with 15% Al_2O_3 has the best superconducting properties. Therefore, further calculations are given based on 15% Al_2O_3-doped YBCO. A larger magnetic moment can be obtained at a lower temperature when the external magnetic field strength is the same. The maximum magnetization of 3D printed samples at 2.5, 4, 15, 35 and 55 K are 5.68, 5.4, 4.19, 1.57 and 0.9 emu g^{-1}, respectively. Compared with the traditional cold-pressed sintered YBCO, 3D-printed YBCO shows considerable improvement in the magnetic moment and hysteresis loops at different temperatures. In figure 4(d), from which YBCO 3D-printing bulk with improved thermal conductivity doped with Al_2O_3nanoparticles also has a transition temperature of 92 K. As is shown in figures 4(e) and (f), at different temperatures (2.5, 4, 15, 35, and 55 K), J_c (H) decreases exponentially with the increase of the magnetic field. The double logarithmic plot of J_c (H) shows an approximately linear relationship to the magnetic field (1000–90 000 Gs) without the so-called fishtail effect. In addition, the power-law relationship between J_c and t is obtained, that is, J_c decreases with the temperature increasing from 0 K to 55 K. After doping with Al_2O_3 nanoparticles, the prepared enhanced 3D printed YBCO superconducting bulk material will have changes in thermal conductivity based on retaining the original superconductivity characteristics.

2.4. Thermal conductivity of Al_2O_3-doped YBCO with high thermal conductivity

Since Al_2O_3 nanoparticles have high thermal conductivity, 3D printed YBCO was doped with 5%, 10% and 15% Al_2O_3 nanoparticles respectively. YBCO high-temperature superconductors are always being used at about 77 K, so the

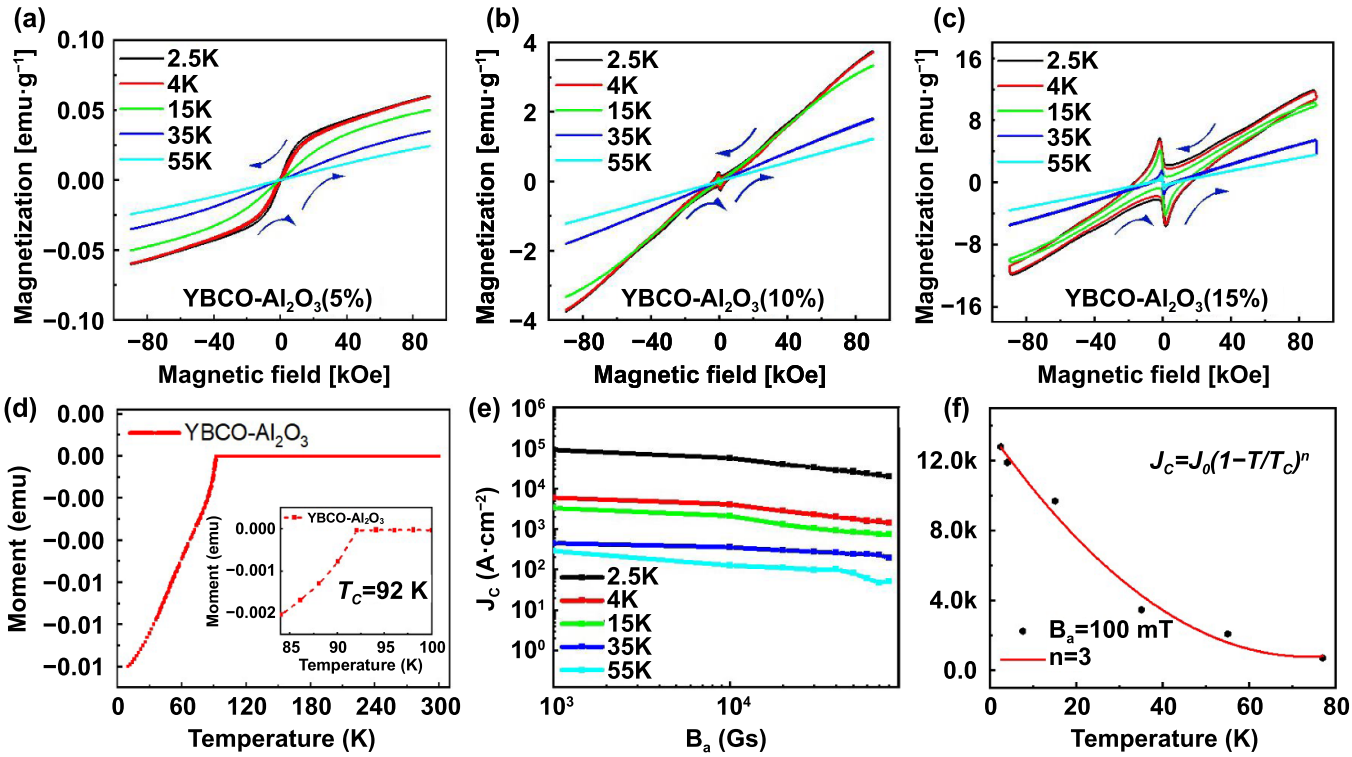

Figure 4. Electromagnetic properties of Al_2O_3-doped thermal enhanced 3D-print YBCO. (a)–(c) Magnetic hysteresis loops of Al_2O_3 doped thermal enhanced 3D-printed sample with 5%, 10% and 15% respectively at 2.5, 4, 15, 35, and 55 K. (d) ZFC and FC curves of Al_2O_3 enhanced sample at an applied field of 50 Oe (inset shows the point of superconducting transition). (e) 3D-printed YBCO J_c (H) with temperature changing from 2.5 K to 55 K. (f) temperature dependence of J_c for $B_a = 100$ mT. The solid line is the fitting curve.

thermal conductivity of undoped and doped YBCO with different proportions was measured from 0 K to 300 K. As shown in figure 5(a), the thermal conductivity of Al_2O_3-doped YBCO doped was improved, and the dependence of thermal conductivity on temperature was a process of first increasing, then decreasing and finally tending to be linear. The change rule of thermal conductivity before and after doping was consistent. Among them, the thermal conductivity of undoped YBCO, YBCO doped with 10% and 15% mass ratio reached the peak value of 16.98, 23.19 and 25.87 W Km^{-1} respectively when the temperature reached 42 K. While the thermal conductivity of samples doped with 10% mass ratio reached the peak value of 22.78 W Km^{-1}, when the temperature reached 62 K. It can be seen that after doping, the thermal conductivity of 3D printed YBCO is improved regardless of the mass ratio of doping. At the same peak period, 3D printed YBCO doped with 10% Al_2O_3nanoparticles has the highest thermal conductivity, whose thermal conductivity is 1.52 times higher than pure YBCO, which has a great influence on the thermal conductivity of YBCO high-temperature superconducting materials. It can also be seen from the figure that after the peak position of the thermal conductivity of the sample, that is, the temperature is 42 K, the improvement of the overall thermal conductivity brought by the doped Al_2O_3nanoparticles with a mass ratio of 5% is the most significant. The improvement of the thermal conductivity of the doped 3D printed YBCO remains 1.5–2 times higher than pure YBCO after 42 K, which can even reach 2.1 times at 300 K. Therefore, the doping mass ratio of Al_2O_3nanoparticles and the improvement of thermal conductivity are not linearly related. In practical engineering applications, it is necessary to select different doping mass fractions of alumina nanoparticles according to the actual working temperature of YBCO high-temperature superconducting materials to achieve the optimal effect. Given the changing trend of thermal conductivity of YBCO high-temperature superconducting materials with temperature increasing first and then decreasing, many researchers have made detailed research and analysis on the mechanism. The existing mechanism explanation is to analyze the influence of phonon heat transfer, electron heat transfer and their coupling effect on thermal conductivity in YBCO at the microscopic level, and then give theoretical formulas for fitting and comparative analysis of experimental data. There is almost no macroscopic model to explain the special change of thermal conductivity of YBCO high-temperature superconducting materials with the temperature rising first and then falling.

As shown in figure 5(b), the 3D printed YBCO samples have a regular porous structure by SEM characterization at room temperature, and through careful observation found that the inner pore structures are mostly regular and irregular hexagons, which are the dominant shape. And the characteristic structure of YBCO is the basis of establishing a macroscopic theoretic model to explain the time dependence of YBCO thermal conductivity. To simplify the model calculation, porous structures inside samples were considered as the same shape at the same temperature. And we assumed these

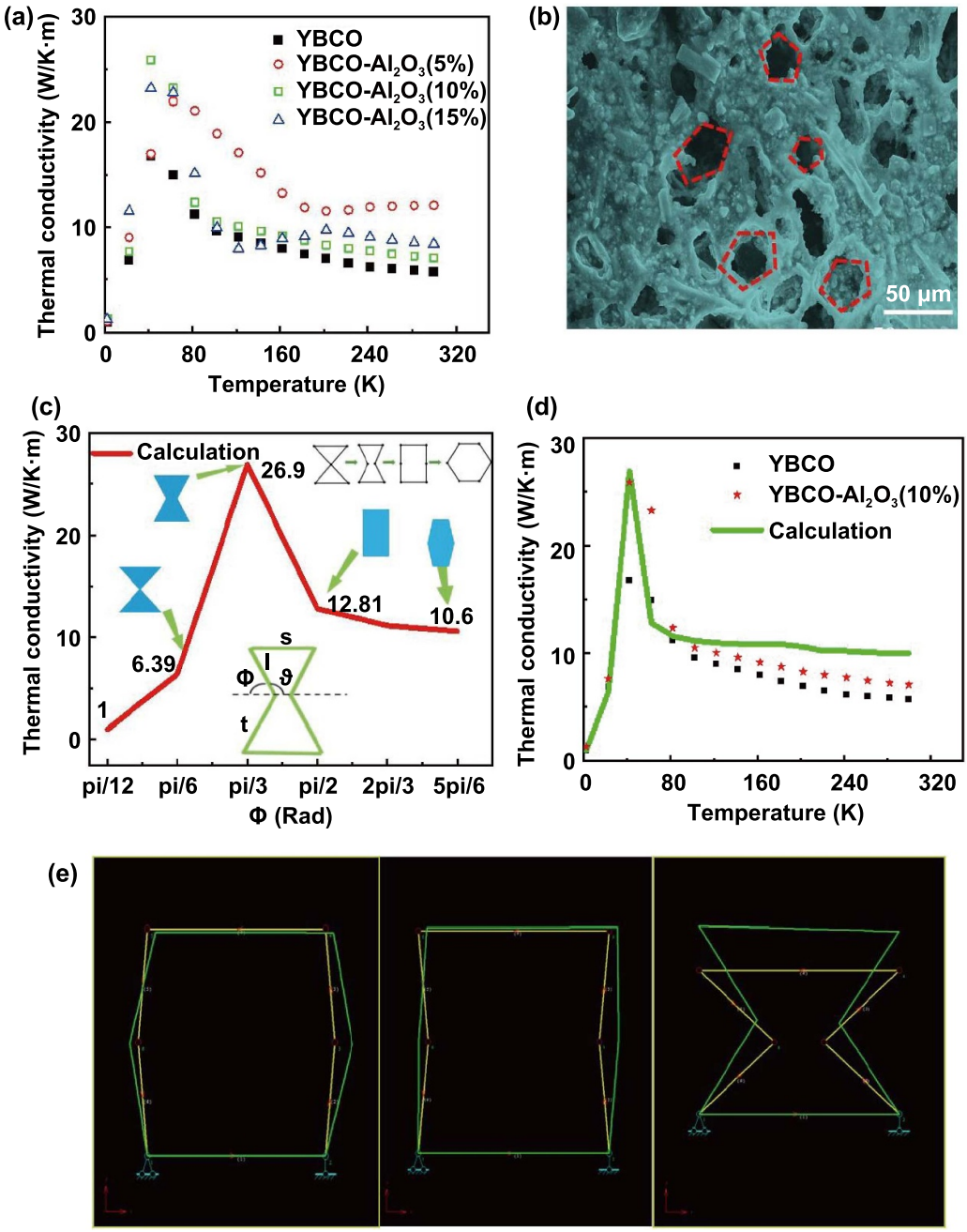

Figure 5. Thermal conductivity of Al_2O_3-doped thermal enhanced 3D-print YBCO. (a) Thermal conductivity of 3D-printed YBCO and Al_2O_3-doped samples with 5%, 10% and 15% doping ratio from 0 to 300 K. (b) SEM image of Al_2O_3-doped samples at room temperature, which shows various kinds of holes with different shapes. (c) Relation between the angle of Φ and the calculating results of the macro model's thermal conductivity. (d) Calculation of macro model based on mechanical deformation compared with experiment results. (e) The deformation of microstructure with the temperature rising. The first one is hexagon, which is at room temperature, the rectangle is at a lower temperature than hexagon, and the last one is at the lowest temperature.

structures as truss structures made up of several hinged bars with the same thickness. In 2008, analytical and finite element methods were used by Bezazi *et al* [35] to analyze the load-bearing and heat-conducting multi-functional applications of a new type of multi-concave honeycomb structure [36]. On this basis, in 2009, Inocenti *et al* [37] established a transient thermal analysis model considering both the thermal radiation and the thermal conduction of solid materials, furthermore, the thermal protection performance of the new honeycomb structure was described [38]. In 2014 [39], based on the Bernoulli–Euler beam model, the Poisson's ratio of honeycomb structure was calculated by using the strain energy principle under pure bending load, on this basis, the influence of the expansion effect of negative Poisson's ratio on the thermal conductivity of the structure is further analyzed [40]. As early as 1935, Bruggeman [41] proposed a new structural model in which

two phases are connected and each phase is continuous. Subsequently, Landauer [42] derived the effective thermal conductivity equation of the structure in 1952. Since most of the voids in 3D printed YBCO were hexagonal at room temperature, the temperature of the YBCO high-temperature Superconductor classification increased from 0 K to 300 K, therefore, it is deduced that the inner structure of the 3D printed sample is hexagonal at room temperature because of the thermal expansion and deformation of the inner structure caused by temperature. The internal structure is a continuous process in which the top-to-top perovskite (structure) of two triangles gradually deforms into a hexagon as the temperature expands. Because the alumina-doped 3D-printing YBCO heat transfer enhancement material is formed by a 3D-printing paste nozzle, the precursor paste is the internal skeleton component of the sintered product, which is itself a porous material. As shown in figure 5(e), the finite element method was used for simulating the structural deformation inside the sample with temperature changing. When the temperature decreases, its structure shrinks, and gradually changes from the initial hexagonal structure to a rectangular structure. Because the rectangular structure itself is unstable, which continues to shrink in the process of continuous temperature decrease, and finally deforms into a special structure with two triangles placed on top. Therefore, our model is based on the porous material as a framework to support the formation of a larger scale of porous materials. Using the heat transfer coefficient formula given by the above researchers, the heat transfer coefficient of 3D printed YBCO light porous material doped with Al_2O_3particles is calculated and the numerical simulation is carried out.

The model calculation is based on the following equations that combine the honeycomb's structural thermal conductivity with the effective thermal conductivity of cellular composite material [36–39]. In the theoretical calculation of the microscopic model, a modified formula has been used as follows to calculate the thermal conductivity of our designed structure with making up of a high thermal conductivity microstructure,

$$k_s = \rho k \tag{2}$$

where k_s represents the sample's conductivity, ρ is a dimensionless value that represents the relative structural density of the model structure, and k denotes the thermal conductivity of the composite material. Next, we give the calculation formula of ρ and k, respectively. Similar to the presentation in the literature [37], we supply one structural influencing factor α, which represents the structural deformation, as shown in the following formula:

$$\rho = \frac{m(n+2)}{2\alpha}\frac{1}{n\sin\theta + \sin\theta\cdot\cos\theta},$$
$$\left(\theta = -\frac{\pi}{120}T + a\pi, m = {}^{t}/_{l}, n = {}^{s}/_{l}\right) \tag{3}$$

where t represents the thickness of model, s and l represent the length of cross rod and sway rod of the model, respectively. T represents the temperature, a is a constant, and θ represents the angle of the model's concave angle which is determined as a function of temperature.

To obtain the thermal conductivity of Al_2O_3-doped YBCO material, we use the formula (4) which has been given in the literature [38, 39] to calculate the thermal conductivity of the composite material with two components,

$$k = \frac{1}{4}\left\{(3v_2-1)k_2 + (3v_1-1)v_1 + \sqrt{\left[(2v_2-1)k_2 + (3v_1-1)k_1\right]^2 + 8k_1k_2}\right\} \tag{4}$$

where v_1, v_2 represent the volume ratio of two main materials, and k_1, k_2 represent two main materials' thermal conductivity. In the end, we obtained the thermal conductivity of the nanoparticle-doped YBCO by the 3D-printing process, which is also fit for other porous materials suitable for 3D-printing,

$$k_s = \frac{m(n+2)}{8\alpha}\frac{\left\{(3v_2-1)k_2 + (3v_1-1)v_1 + \sqrt{\left[(2v_2-1)k_2 + (3v_1-1)k_1\right]^2 + 8k_1k_2}\right\}}{n\sin(-\frac{\pi}{120}T + a\pi) + \sin(-\frac{\pi}{120}T + a\pi)\cdot\cos(-\frac{\pi}{120}T + a\pi)}. \tag{5}$$

As shown in figure 5(c), the inside microstructure of the sample changed with different Φ values since the structure we put forward has changed with the temperature rising (As shown in figure S2, supporting information). It is clear that when the Φ is about 60°, the sample's thermal conductivity reached its peak value. As shown in figure 5(d), the green lines represent the numerically calculated results of the temperature dependence of the thermal conductivity of the 10% Al_2O_3-doped YBCO sample on the macroscopic scale model we have established, and the red asterisks represent 3D printed YBCO samples doped with 10% Al_2O_3 nanoparticles, the black squares represent the undoped 3D printed YBCO samples. It can be seen that our macroscopic theoretic model based on thermal expansion-induced structural deformation can well explain the unique temperature dependence of the thermal conductivity of 3D printed YBCO superconductor classification in doped or undoped conditions. Since we assumed structures inside samples are all the same shape at the same temperature and assumed the density of samples is 100%, there is a difference between the experimental results and theoretical calculation, which is acceptable.

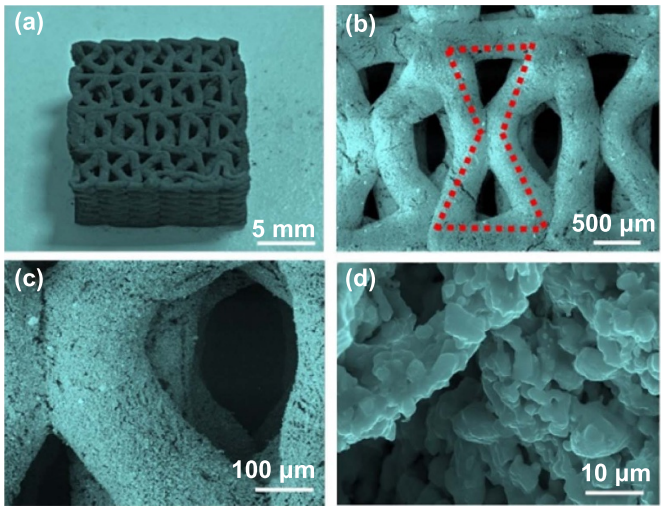

Figure 6. Microstructural characterization of designed Al_2O_3-doped 3D-printed YBCO. (a) Optical image of designed 3D-printed YBCO with larger thermal conductivity structure. (b)–(d) SEM images of designed 3D-printed YBCO with a high thermal conductivity structure, which is also a porous structure.

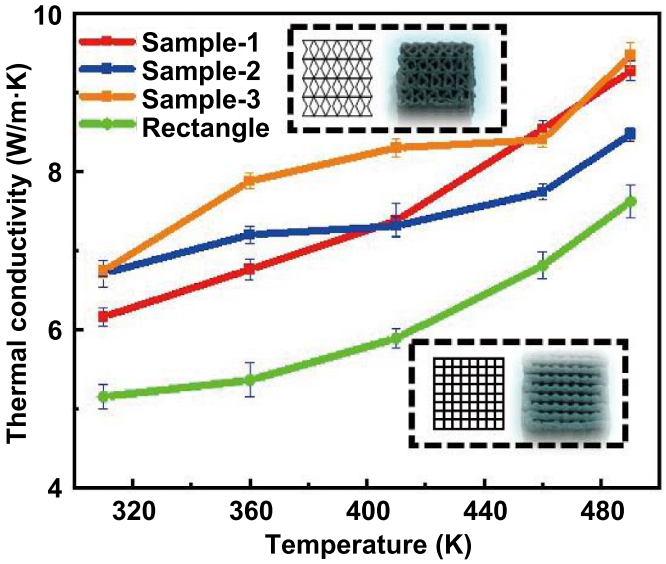

Figure 7. Designed controllable structure made of YBCO with high thermal conductivity compared with conventional rectangle 3D-printed structure.

2.5. Controllable designed 3D-printed YBCO structure with high thermal conductivity

As mentioned above, a macroscopic theoretic model has been established based on the thermal expansion deformation of the frame structure to calculate the thermal conductivity of the macroscopic structure. When the thermal conductivity reaches its peak, the inner structure is shown as a concave hexagon. And through our calculation of the thermal conductivity of the model, it can be concluded that when the thermal conductivity of the sample reaches its peak, the concave angle of the structure is 120°. Therefore, with the help of the results of calculation and analysis, the DIW 3D-printing YBCO technology has been used to directly design and print the YBCO structure with the largest thermal conductivity in the range of 0–300 K. As shown in figure 6(a), for the YBCO bulk with high thermal conductivity fabricated by 3D-printing technique, the YBCO exhibited a regular periodic structure, these structures are formed by the deposition of cylindrical slurry from a nozzle with an inner diameter of about 200 μm, which is set up according to the procedure of the printing model. Because the prepared ceramic printing paste has excellent rheological properties, it can be successfully extruded without powder agglomeration, which allows the geometry to be accurately copied from the structure so that 3D-printed samples can be made accurately. As shown in figures 6(c) and (d). The rod-like structure of 3D printed YBCO is also porous, so the YBCO bulk with high thermal conductivity retained its ultra-light property. As shown in figure 7, we tested the thermal conductivity of both YBCO bulks with vertical and horizontal orthogonal deposition printed by Zhang *et al* [30], and YBCO bulks with designed structure in the normal temperature section. It has been found that the thermal conductivity of three YBCO bulks with optimized structures was significantly improved compared with that of YBCO blocks with a square grid, and all of the samples are undoped with Al_2O_3. At temperature of 360 K, the maximum thermal conductivity of the designed structure can reach 1.47 times that of the square grid structure. Therefore, a structural design method of controllable thermal conductivity based on 3D-printing technology has been confirmed from the experimental point of view, and the functional YBCO 3D-printed structural composite material has been successfully prepared, which provides a high reference value for the later practical application.

3. Conclusions

In this paper, based on 3D-printing technology, on one hand, by doping Al_2O_3 nanoparticles with high thermal conductivity into the precursor printing paste, high-quality nano-doping has been realized. And the results show that the thermal conductivity of superconducting materials has been increased up to 2 times. By analyzing its microstructure and combining it with the theoretical calculation model, the calculation results are in good agreement with the experiments, and a microstructure with high thermal conductivity has also been found. On this basis, another major task of this paper is to prepare macroscopic samples with this microstructure with high thermal conductivity by 3D-printing. The results show that this structural design can also effectively improve thermal conductivity, and the maximum thermal conductivity can reach almost 1.5 times. This new method of improving thermal conductivity through paste doping and structural design proposed is also applicable to other porous materials that can be prepared by the 3D-printing process.

Data availability statement

Research data are not shared.

Acknowledgments

One of the authors (X Y Zhang) thanks Professor Q Q Zhang (Lanzhou University, China) and Professor T Suo (Northwestern Polytechnical University, China) for their kind help. This work is supported by the Fund of Natural Science Foundation of China (No. 11872196, 12232005). This study is financially supported by the Outstanding Postgraduate 'Innovation Star' Fund for Distinguished of Gansu Province (No. 2021CXZX-032).

Conflict of interest

The authors declare no conflict of interest.

ORCID iD

Xingyi Zhang https://orcid.org/0000-0003-2856-170X

References

[1] Uher C 1990 Thermal conductivity of high-T_c superconductors *J. Supercond.* **3** 337–89
[2] Terzijska B M, Wawryk R, Dimitrov D A, Marucha C, Kovachev V T and Rafalowicz J 1992 Thermal conductivity of YBCO and thermal conductance at YBCO/ruby boundary part 1: joint experimental set-up for simultaneous measurements and experimental study in the temperature range 10–260 K *Cryogenics* **32** 53–59
[3] Zeini B, Freimuth A, Büchner B, Galffy M, Gross R, Kampf A P, Kläser M, Müller-Vogt G and Winkler L 2001 Thermal conductivity and thermal hall effect in Bi- and Y-based high-T_c superconductors *Eur. Phys. J.* B **20** 189–208
[4] Ausloos M 2001 Electrical and thermal transport properties in high T_c superconductors: effects of a magnetic field *Phys.* C **354** 160–4
[5] Su X Y , Liu C, Zhou J, Zhang X Y and Zhou Y H 2020 A method to access the electro-mechanical properties of superconducting thin film under uniaxial compression *Acta Mech. Sin.* **36** 1046–50
[6] Tewordt L and Wölkhausen T 1989 Theory of thermal conductivity of the lattice for high-T_c superconductors *Solid State Commun.* **70** 839–44
[7] Regueiro M D N and Castello D 1991 Thermal conductivity of high temperature superconductors *Int J. Mod. Phys.* B **5** 2003–35
[8] Jing Z 2016 Coupled multiphysics modeling of the thermal-magnetic-mechanical instability behavior in bulk superconductors during pulsed field magnetization *Supercond. Sci. Technol.* **29** 105001
[9] Jing Z, Yong H D and Zhou Y H 2016 Influences of non-uniformities and anisotropies on the flux avalanche behaviors of type-II superconducting films *Supercond. Sci. Technol.* **29** 105001
[10] Jing Z, Yong H D and Zhou Y H 2015 Dendritic flux avalanches and the accompanied thermal strain in type-II superconducting films: effect of magnetic field ramp rate *Supercond. Sci. Technol.* **28** 075012
[11] Jing Z and Ainslie M D 2020 Numerical simulation of flux avalanches in type-II superconducting thin films under transient AC magnetic fields *Supercond. Sci. Technol.* **33** 084006
[12] Jing Z 2020 Numerical modelling and simulations on the mechanical failure of bulk superconductors during magnetization: based on the phase-field method *Supercond. Sci. Technol.* **33** 075009
[13] Jezowski A, Mucha J and Pompe G 1987 Thermal conductivity of the amorphous alloy $Fe_{40}Ni_{40}P_{14}B_6$ between 80 and 300 K *J. Phys. D: Appl. Phys.* **20** 1500–6
[14] Uher C and Kaiser A B 1987 Thermal transport properties of $YBa_2Cu_3O_7$ superconductors *Phys. Rev.* B **36** 5680–3
[15] Morelli D T, Heremans J and Swets D E 1987 Thermal conductivity of superconductive Y–Ba–Cu–O *Phys. Rev.* B **36** 3917–9
[16] Ikebe M, Fujishiro H, Naito T, Noto K, Kohayashi S and Yoshizawa S 1994 Thermal conductivity of YBCO(123) and YBCO(211) mixed crystals prepared by MMTG *Cryogenics* **34** 57–61
[17] Peacor S D, Cohn J L and Uher C 1991 Effect of magnetic field on thermal conductivity of $YBa_2Cu_3O_{7-\delta}$ single crystals *Phys. Rev.* B **43** 8721–4
[18] Hull J R 1989 High temperature superconducting current leads for cryogenic apparatus *Cryogenics* **29** 1116–23
[19] Salama K, Selvamanickam V, Gao L and Sun K 1989 High current density in bulk $YBa_2Cu_3O_x$ superconductor *Appl. Phys. Lett.* **54** 2352–4
[20] Flik M I and Tien C L 1990 Size effect on the thermal conductivity of high-T_c thin-film superconductors *J. Heat Transfer* **112** 872–81
[21] Li Y B, Ma Y B, Liu C, Zhang X Y, Yong H D and Zhou Y H 2021 Fluorescent paint for determination on the effective thermal conductivity of YBCO coated conductor *Supercond. Sci. Technol.* **34** 035029
[22] Castellazzi S, Cimberle M R, Ferdeghini C, Giannini E, Grasso G, Marrè D, Putti M and Siri A S 1997 Thermal conductivity of a BSCCO(2223) c-oriented tape: a discussion on the origin of the peak *Phys.* C **273** 314–22
[23] Yamamoto H, Sano M, Ozawa S, Tanaka M, Kaneko M, Matsubara Y and Ogasawara T 1991 Thermal conductivity of high T_c YBaCuO bulk prepared by melt growth technique *Supercond. Sci. Technol.* **4** S355–257
[24] Rodríguez J E 2008 Ag-YBCO compounds as thermoelectric material *Phys. Status Solidi* a **205** 1173–6
[25] Diko P 2004 Cracking in melt-grown Re-Ba-Cu-O single-grain bulk superconductors *Supercond. Sci. Technol.* **17** R45–R58
[26] Diko P and Krabbes G 2003 Macro-cracking in melt-grown YBaCuO superconductor induced by surface oxygenation *Supercond. Sci. Technol.* **16** 90–93
[27] Surjadi J U, Feng X B, Zhou W Z and Lu Y 2021 Optimizing film thickness to delay strut fracture in high-entropy alloy composite microlattices *Int. J. Extrem. Manuf.* **3** 025101
[28] Zhang W Q, Ye H T, Feng X B, Zhou W Z and Cao K 2022 Tailoring mechanical properties of PμSL 3D-printed structures via size effect *Int. J. Extrem. Manuf.* **4** 045201
[29] Sun Q S, Xue Z X, Chen Y, Xia R D, Wang J M, Xu S, Zhang J and Yue Y N 2021 Modulation of the thermal transport of micro-structured materials from 3D printing *Int. J. Extrem. Manuf.* **4** 015001
[30] Zhang B Q, Zhang Q Q, He P, Ma Y B, Shen L, Zhang X Y and Zhou Y H 2021 Efficient fabrication of ultralight $YBa_2Cu_3O_{7-x}$ superconductors with programmable shape and structure *Adv. Funct. Mater.* **31** 2100680
[31] Wang X F, Sun Y H, Peng C Q, Luo H, Wang R C and Zhang D 2015 Transitional suspensions containing thermosensitive dispersant for three-dimensional printing *ACS Appl. Mater. Interfaces* **7** 26131–6

[32] Deville S, Saiz E, Nalla R K and Tomsia A P 2006 Freezing as a path to build complex composites *Science* **311** 515–8
[33] Sun K, Wei T S, Ahn B Y, Seo J Y, Dillon S J and Lewis J A 2013 3D printing of interdigitated Li-ion microbattery architectures *Adv. Mater.* **25** 4539–43
[34] Bean C P and Schmitt R W 1963 The physics of high-field superconductors: new materials, used in lossless magnets at low temperatures, challenge scientific understanding *Science* **140** 26–35
[35] Bezazi A, Remillat C, Innocenti P and Scarpa F 2008 In-plane mechanical and thermal conductivity properties of a rectangular–hexagonal honeycomb structure *Compos. Struct.* **84** 248–55
[36] Bezazi A, Scarpa F and Remillat C 2005 A novel centresymmetric honeycomb composite structure *Compos. Struct.* **71** 356–64
[37] Innocenti P and Scarpa F 2009 Thermal conductivity properties and heat transfer analysis of multi-re-entrant auxetic honeycomb structures *J. Compos. Mater.* **43** 2419–39
[38] Wu J Y, Chen F, Shen Q and Zhang L M 2011 Effect of thermal conductivity and analytical calculation method of effective thermal conductivity for porous ceramics *Adv. Ceram.* **32** 13–16
[39] Hou X H and Yin G S 2014 Heat transfer performance for a new honeycomb structure *J. Hebei Univ. Technol.* **43** 72–76
[40] Gu S and Evans A G 2001 On the design of two-dimensional cellular metals for combined heat dissipation and structural load capacity *Int. J. Heat Mass Transfer* **44** 2163–75
[41] Bruggeman D A G 1935 Berechnung verschiedener physikalischer Konstanten von heterogenen Substanzen. I. Dielektrizitätskonstanten und leitfähigkeiten der mischkörper aus isotropen substanzen *Ann. Phys.* **416** 665–79
[42] Landauer R 1952 The electrical resistance of binary metallic mixtures *J. Appl. Phys.* **23** 779–91